Pergamon

Int. J. Heat Mass Transfer. Vol. 39, No. 11, pp. 2311–2317, 1996

0017-9310/96 $15.00 + 0.00

0017-9310(95)00307-X

Thin-film-heater thermal conductivity apparatus and measurement of thermal conductivity of silica aerogel

J. S. Q. ZENG, P. C. STEVENS and A. J. HUNT
Lawrence Berkeley Laboratory, University of California, Berkeley, CA 94720, U.S.A.

R. GRIEF
Department of Mechanical Engineering, University of California, Berkeley, CA 94720, U.S.A.

and

DAEHEE LEE
Department of Mechanical Engineering, Inje University, Kimhae Kyongnam, Korea

(*Received* 29 *December* 1994 *and in final form* 7 *August* 1995)

Abstract—An apparatus was developed for the measurement of thermal conductivity under steady conditions. The apparatus uses a 10 nm thick gold film heater that is coated on a polyester sheet. The important advantages of this heater are spatial uniformity of the heat generation and a small thickness. The apparatus is compact and has only a small edge loss of heat. The apparatus was used to measure the thermal conductivity of silica aerogel. The heat transfer modes in silica aerogel include gas and solid conduction and thermal radiation. The experiments provide results for the total heat transfer and hence, total (apparent) thermal conductivity. The separate solid and radiative contributions were obtained from analyses of the energy transfer. The solid conductivity of silica aerogel varies with temperature more slowly than the radiative conductivity does. The Rosseland absorption coefficient of silica aerogel decreases with temperature. Assuming one-dimensional heat transfer, the uncertainty of the results for the thermal conductivity is about 5.5%. A three-dimensional analysis is used to evaluate the validity of the assumption of one-dimensional heat transfer in the apparatus. The results shows that the assumption of one-dimensional heat transfer in the apparatus results in a reduction of the thermal conductivity of 1.7% at 20°C and a 7.3% reduction at 90°C. Copyright © 1996 Elsevier Science Ltd.

INTRODUCTION

The thermal conductivity, k, of a homogeneous material is often determined under steady state conditions assuming one dimensional transport, i.e.

$$k = q \cdot \delta/(T_2 - T_1). \quad (1)$$

One difficulty in accurately determining the thermal conductivity is in attaining one-dimensional heat transfer; this requires a very large planar heat source and sample. However, for large systems a long time is required to achieve steady state conditions; in addition, samples of large size are often not available. hence, it is advantageous to have a thin heater and a thin sample. This paper describes a thermal conductivity apparatus which employs a thin film heater.

A number of thin-heater thermal conductivity systems have been developed. Hager [1] reported on an apparatus which uses a 102×305 cm^2, 0.03 mm thick no. 321 stainless steel foil as a heater. The thickness of the foil is uniform to within $\pm 2\%$. Thermocouple platelets are enclosed between two 102×152 mm^2 sheets of 0.25 mm thick silicone–glass laminate. These platelets and their leads are electrically insulated from each other with a 0.05 mm polyimide film. McElroy *et al.* [2] reported on an apparatus which uses a Nichrome metal-screen heater. The screen was made from 0.25-mm-diameter wire woven on a 40 by 40 mesh (per in) and has a thickness of 0.64 mm, a width of 0.914 m and a length of 1.52 m. The screen is held in a frame with 14 electrically insulated tension springs with adjustable nuts. Type E thermocouples, 0.12 mm in diameter, are attached to the screen with thermally conducting epoxy.

The present work utilizes a gold film heater of 10 nm thickness coated on a polyester film. The advantages of this heater include spatial uniformity of the heat generation and small thickness. The small thickness of the heater makes the apparatus compact with a small edge loss of heat.

It is expected that the assumption of one-dimensional heat transfer is valid in the central region of the apparatus. Thermocouples are placed near the centre, where the temperatures of the heater and the cold plate are measured. If the local heat flux in the central

NOMENCLATURE

a_λ	absorption coefficient [$m^2\ kg^{-1}$]
a_R	Rosseland absorption coefficient [$m^2\ kg^{-1}$]
A	defined in equation (5)
B	defined in equation (5)
$e_{b\lambda}$	spectral emissive power
e_b	total emissive power
F	heater area [cm^2]
I	electric current [A]
I_λ	radiation intensity
k_{app}	total apparent thermal conductivity [$W\ m^{-1}\ K^{-1}$]
k_c	solid and gas conductivity [$W\ m^{-1}\ K^{-1}$]
k_r	radiative thermal conductivity [$W\ m^{-1}\ K^{-1}$]
L_x, L_y, L_z	length, width and thickness of test sample [cm]
n	refractive index
N	conduction-radiation parameter, defined in equation (11)
q	heat flux [$W\ m^{-2}$]
Q	heating power of heater [W]
q_c	heat flux due to conduction [$W\ m^{-2}$]
q_r	heat flux due to radiation [$W\ m^{-2}$]
$q_{r,\xi}$	radiative heat flux in ξ direction [$W\ m^{-2}$]
T	temperature [K]
T_{amb}	ambient temperature [K]
V	voltage [V].

Greek symbols

δ	thickness of test sample ($=L_z$) [cm]
ε	emissivity
λ	wavelength [μm]
σ	Stefan–Boltzmann constant
Ψ	slip coefficient, defined in equation (10a–f).

Subscripts

app	apparent
b	blackbody
w	wall
λ	wavelength.

region were known, an accurate determination of the thermal conductivity could be made from equation (1). However, only the total (or average) heat flux is obtained from the total power. Replacing the local heat flux in equation (1) with the average heat flux introduces some error. To assess the error, three-dimensional energy transfer is studied.

The apparatus has been used to determine the thermal conductivity of a porous medium, namely, silica acrogel. Silica aerogel is a highly porous, open-cell foam material made by supercritical extraction of the interstitial liquid from the voids of a colloidal gel of silica [3]. The nanosized cells/pores and particles which make up aerogels are primarily responsible for their very low thermal conductivity. The heat transfer modes in aerogel include gas and solid conduction and thermal radiation. The experiments provide a total (apparent) thermal conductivity. Energy transfer due to gas conduction can be determined by carrying out the experiments at a very low gas pressure (e.g. below 1 Torr). At low pressure (below 1 Torr) the energy transfer due to gas conduction is negligible compared with the other two modes and the total transfer essentially results from the solid and radiation contributions. The solid and radiative contributions are independent of the pressure and so the gas conduction at higher pressures can then be obtained by subtracting this measured result (for the solid and radiative heat transfer) from the total heat transfer (at higher pressures). It is difficult, however, to obtain the separate energy transfer contributions due to solid conduction and to radiation for a radiatively participating medium. Note that for silica aerogel, even at ambient temperature, the solid and radiative heat transfer are of the same magnitude. In this work the solid conduction and radiative transfer contributions are each determined in a three-dimensional analysis.

EQUIPMENT DESCRIPTION

The apparatus consists of a thin-film heater, cold plates and temperature control bath, vacuum chamber and vacuum pump and data acquisition system. The gold film heater is coated on a polyester sheet 25.4 cm square and 0.12 mm thick. It is attached on the gold side to a 0.08 mm thick polyester sheet 31.8 cm square. The gold film is protected by an electrically conductive coating that permits direct attachment of electrical bus bars to the film. The temperature of the heater is maintained by adjusting the direct current voltage that is applied across the heater using a Lambda LP-520-FM power supply. The heater current is determined by measuring the voltage across a 50 milli-Ohm shunt in series with the heater. The heater voltage is measured using a Hewlett Packard 3468B digital multimeter at voltage taps on the heater bus bars with leads separate from the power leads.

The cold plates are made of copper, 32.4 cm square and 1.3 cm thick, with 0.6 cm copper tubing brazed onto the external surface to carry cooling water. The surfaces facing the samples have been machined to a flatness of ± 0.08 mm. The plates are held by four

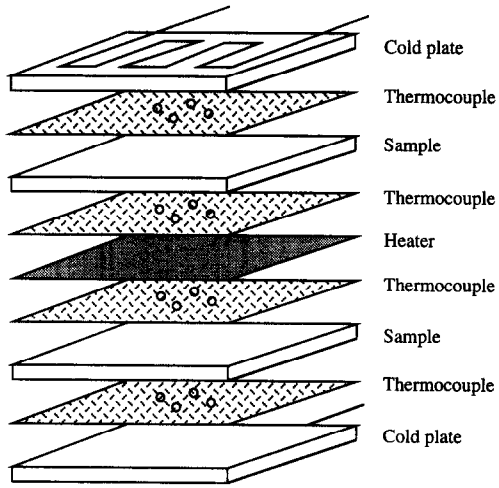

Fig. 1. Schematic assembly of thermal conductivity apparatus showing the copper plates, sample arrangement and distribution of thermocouples.

threaded rods that run through insulating washers in holes in the corners. The temperature of the cold plates is maintained by circulating water from a Neslab RTE 110 temperature control bath.

A vacuum system permits measurement of the pressure dependence of thermal conductivity of aerogel. The experimental assembly consisting of the heater, test samples and copper plates (Fig. 1) is mounted inside a vacuum chamber fitted with electrical and coolant conduits. The system is capable of achieving gas pressures in the chamber from less than 1 Torr to ambient.

The temperatures are measured using 16 Type E (Chromel P constantan) 0.13 mm diameter thermocouples mounted to 0.13 mm thick polyester sheets with 0.08 mm Kapton tape. There are four thermocouples for each surface of the samples arranged 2.5 cm from the center. The thermocouples are monitored with a computer using a 16 channel 16 bit data acquisition system. The thermocouple system was calibrated using a platinum resistance temperature device whose output had been calibrated to a platinum resistance thermometer traceable to NIST. 16 thermocouples were mounted on the heater to measure the temperature distribution. Figure 2a shows the heater temperature distribution with no power applied and with the cold plate temperature maintained at 10°C. Figure 2b shows the heater temperature distribution with power applied and with the cold plates at 10°C. One-cm-thick aerogel samples were used in the measurements. It is seen that the central region (with a diameter of about 15 cm) of the heater has a temperature variation of 0.5°C. Near the edge the heater has 2–3°C lower temperature because of the edge heat loss. This is also true when the cold plates are maintained at 80°C. The experiment showed that a variation of the cold plate temperature with a mean 10°C was 0.2°C. Figure 2c shows how the 16 thermocouples

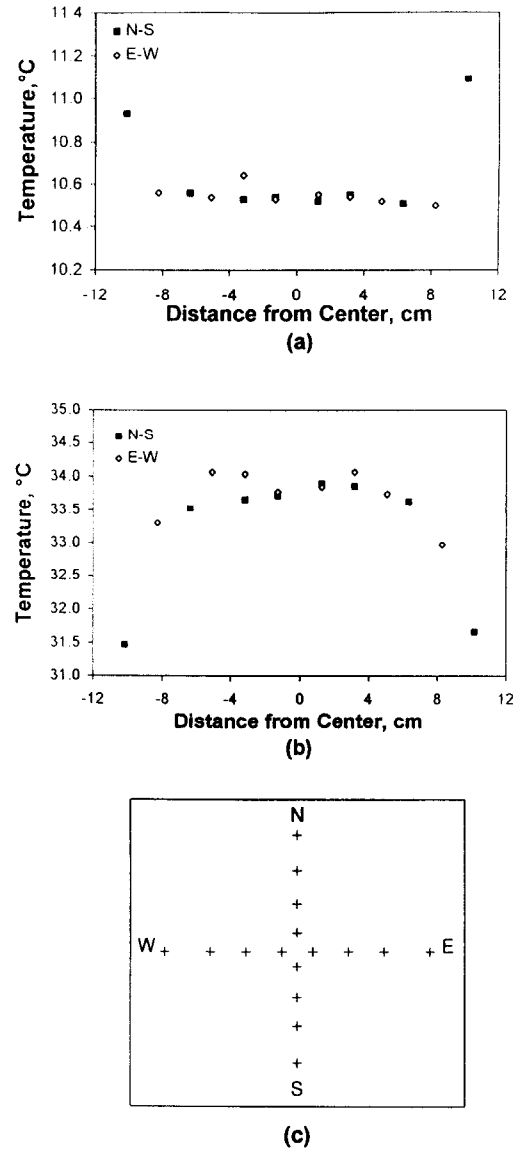

Fig. 2. (a) Temperature distribution on the heat surface with no power to the heater, (b) temperature distribution on the heater surface with 3.76 W of power, (c) a schematic of the thermocouple distribution for the test of temperature uniformity.

were arranged on the heater to obtain these measurements.

MEASUREMENT OF THERMAL CONDUCTIVITY AND ABSORPTION COEFFICIENT OF AEROGEL

Bulk fused silica is opaque at about 9 and 21 μm due to the fundamental Si-O molecular vibrations; aerogel, which is composed primarily of silica and air, also absorbs strongly in these spectral regions. However, in the 3–6 μm range, aerogel is almost transparent. To eliminate this infrared window, carbon can be loaded into the aerogel either as a fine powder

mixed into the gel solution or by chemical vapor infiltration after drying.

The pair of aerogel samples measured were $25.4 \times 25.4 \times 1.16$ cm^3 each with a density of 0.096 g cm^{-3} and 12% by weight carbon loading. The paired samples were placed in the thermal conductivity apparatus. A border of aerogel of the same thickness was added to extend 3 cm beyond the edge of the heater to reduce the lateral heat transfer. To ensure good thermal contact, the samples were compressed by the copper plates to about 5% strain. The measurements were made at different gas pressures and different mean sample temperatures.

To validate this thin-film-heater thermal conductivity apparatus, the thermal conductivity of an opacified aerogel was evaluated with this apparatus and also evaluated in accordance with ASTM C 177-85 utilizing a Holometrix Model TCFGM guarded hot plate apparatus [4]. The thermal conductivity of the aerogel measured from the two apparatuses differs by 1% at 2 Torr gas pressure and 3.8% at ambient pressure.

Thin samples (about 0.1–0.3 mm) of aerogel were prepared for spectrophotometric infrared measurement. Transmission data were used to calculate the specific spectral absorption coefficient, a_λ, by using Beer's law, $I_\lambda(x)/I_{0_\lambda} = \exp(-a_\lambda \rho x)$. Results obtained for a_λ are listed in Table 1.

HEAT TRANSFER ANALYSIS

The steady state energy equation for a participating medium with no internal heat generation is [5]

$$-\nabla\cdot(q_r+q_c) = -\left(\frac{\partial q_{r,x}}{\partial x}+\frac{\partial q_{r,y}}{\partial y}+\frac{\partial q_{r,z}}{\partial z}\right) + k_c\left(\frac{\partial^2 T}{\partial x^2}+\frac{\partial^2 T}{\partial y^2}+\frac{\partial^2 T}{\partial z^2}\right)=0 \quad (2)$$

where

$$\frac{\partial q_{r,\xi}}{\partial \xi} = \int_{\lambda=0}^{\infty} \frac{\partial q_{r\lambda,\xi}}{\partial \xi} d\lambda, \quad \xi = x, y, z. \quad (3)$$

For an optically thick medium, the diffusion approximation can be used, i.e.

$$q_{r\lambda,\xi} = -\frac{4}{3a_\lambda}\frac{\partial e_{b\lambda}}{\partial \xi}, \quad \xi = x, y, z \quad (4)$$

where a_λ is the spectral absorption coefficient. Substituting equation (4) into equation (3) yields

$$\frac{\partial q_{r,\xi}}{\partial \xi} = -A\left(\frac{\partial T}{\partial \xi}\right)^2 - B\frac{\partial^2 T}{\partial \xi^2}$$

$$A = \frac{4}{3}\int_0^\infty \frac{1}{a_\lambda}\frac{\partial^2 e_{b\lambda}}{\partial T^2} d\lambda \quad B = \frac{4}{3}\int_0^\infty \frac{1}{a_\lambda}\frac{\partial e_{b\lambda}}{\partial T} d\lambda, \quad (5a)$$

where

$$\frac{\partial e_{b\lambda}}{\partial T} = \frac{2\pi C_1 C_2}{n^3 \lambda^6 T^2}\frac{\exp(C_2/n\lambda T)}{[\exp(C_2/n\lambda T)-1]^2}$$

$$\left(C_1 = 0.59544 \times 10^8 \frac{\text{W}\,\mu\text{m}^4}{\text{m}^2}; \quad C_2 = 14\,388\,\mu\text{m}\cdot\text{K}\right), \quad (5b)$$

Table 1. Absorption coefficients of opacified silica aerogel

λ, μm	a_λ, m^2 kg^{-1}	λ, μm	a_λ, m^2 kg^{-1}	λ, μm	a_λ, m^2 kg^{-1}	λ, μm	a_λ, m^2 kg^{-1}
2.5	18.26	4.8	7.29	7.1	13.62	9.4	823.4
2.6	18.26	4.9	8.47	7.2	14.63	9.5	769.1
2.7	35.41	5.0	10.20	7.3	16.14	9.6	619.4
2.8	32.64	5.1	10.88	7.4	19.02	9.7	522.6
2.9	28.05	5.2	11.05	7.5	25.17	9.8	431.5
3.0	21.20	5.3	13.04	7.6	30.74	9.9	318.6
3.1	17.05	5.4	13.82	7.7	35.23	10	275.6
3.2	14.4	5.5	12.29	7.8	50.86	10.5	283.8
3.3	13.23	5.6	11.05	7.9	70.43	11.0	221.7
3.4	11.75	5.7	10.54	8.0	150.5	11.5	180.3
3.5	10.87	5.8	10.54	8.1	170.3	12.0	173.8
3.6	10.37	5.9	10.88	8.2	250.3	12.5	236.4
3.7	9.41	6.0	11.93	8.3	350.3	13.0	187.0
3.8	9.40	6.1	13.23	8.4	460.3	13.5	167.3
3.9	8.93	6.2	13.82	8.5	480.7	14.0	167.4
4.0	8.47	6.3	13.82	8.6	500.7	14.5	167.4
4.1	8.32	6.4	12.66	8.7	619.4	15.0	173.8
4.2	8.17	6.5	12.11	8.8	800.4	15.5	180.3
4.3	8.17	6.6	12.11	8.9	890.2	16.0	193.7
4.4	7.87	6.7	12.11	9.0	1100.5	17.0	200.5
4.5	7.58	6.8	12.29	9.1	1200.1	18.0	210.3
4.6	7.44	6.9	12.48	9.2	1130.4	19.0	230.6
4.7	7.29	7.0	13.04	9.3	923.4	20.0	243.8

$$\frac{\partial^2 e_{b\lambda}}{\partial T^2} = \frac{2\pi C_1 C_2}{n^3 \lambda^6 T^4} \times \frac{\{(C_2/n\lambda)[\exp(C_2/n\lambda T)+1]-2T \times [\exp(C_2/n\lambda T)-1]\}\exp(C_2/n\lambda T)}{[\exp(C_2/n\lambda T)-1]^3}. \quad (5c)$$

The refractive index, n, in the above equation has a value of about 1.03 for silica aerogel [6]. Substituting equation (5) into equation (2) yields

$$A\left[\left(\frac{\partial T}{\partial x}\right)^2+\left(\frac{\partial T}{\partial y}\right)^2+\left(\frac{\partial T}{\partial z}\right)^2\right] + (B+k_c)\left(\frac{\partial^2 T}{\partial x^2}+\frac{\partial^2 T}{\partial y^2}+\frac{\partial^2 T}{\partial z^2}\right)=0. \quad (6)$$

Using the Rosseland mean absorption coefficient, a_R, and the radiative conductivity, k_r,

$$\frac{1}{a_R} = \int_0^\infty \frac{1}{a_\lambda}\frac{\partial e_{b\lambda}}{\partial e_b}\,d\lambda, \quad k_r = \frac{16\sigma T^3}{3a_R}, \quad (7)$$

the radiative flux vector can be written as

$$q_r = -\frac{4}{3a_R}\nabla e_b = -\frac{16\sigma T^3}{3a_R}\nabla T = -k_r \nabla T. \quad (8)$$

The energy equation is

$$-\nabla\cdot(q_r+q_c) = \frac{\partial}{\partial x}\left[(k_r+k_c)\frac{\partial T}{\partial x}\right] + \frac{\partial}{\partial y}\left[(k_r+k_c)\frac{\partial T}{\partial y}\right]+\frac{\partial}{\partial z}\left[(k_r+k_c)\frac{\partial T}{\partial z}\right]=0. \quad (9)$$

It is often convenient to use equation (6) instead of equation (9) because k_r is a complicated function of temperature.

To obtain the temperature distribution, equation (6) must be solved subject to the imposed specified temperatures on the surfaces of the aerogel sample. However, equation (6), which uses the diffusion approximation, is not valid near a boundary. Consequently, it cannot be used directly with the boundary conditions. To overcome this difficulty, the boundary conditions are modified. The thin-film-heater and copper plates are opaque to infrared radiation. The four lateral sides are treated as black at ambient temperature. The effective boundary conditions can be written as [7]

$$\Psi(0,y,z) = 4\sigma T_{amb}^3[T_{amb}-T(0,y,z)]/q_{r,x}(0,y,z) \quad (10a)$$

$$\Psi(L_x,y,z) = 4\sigma T_{amb}^3[T(L_x,y,z)-T_{amb}]/q_{r,x}(L_x,y,z) \quad (10b)$$

$$\Psi(x,0,z) = 4\sigma T_{amb}^3[T_{amb}-T(x,0,z)]/q_{r,y}(x,0,z) \quad (10c)$$

$$\Psi(x,L_y,z) = 4\sigma T_{amb}^3[T(x,L_y,z)-T_{amb}]/q_{r,y}(x,L_y,z) \quad (10d)$$

$$\Psi(x,y,0) = 4\sigma T_{w,z=0}^3[T_w(x,y,0) - T(x,y,0)]/q_{r,z}(x,y,0) \quad (10e)$$

$$\Psi(x,y,L_z) = 4\sigma T_{w,z=L_z}^3[T(x,y,L_z) - T_w(x,y,L_z)]/q_{rz}(x,y,L_z), \quad (10f)$$

where the slip coefficient, Ψ, is given by

$$\Psi(x,y,z) = [1/\varepsilon(x,y,z)-1/2]/[1+3N(x,y,z)/4],$$

$$N(x,y,z) = k_c a_R/4\sigma T(x,y,z)^3 = 4k_c/3k_r(x,y,z). \quad (11)$$

The emissivity of mylar on copper and mylar on gold is 0.365 [8]. An additional boundary condition on the side of the heater is

$$q_z(x,y,0) = -[k_r(x,y,0)+k_c]\partial T(x,y,0)/\partial z. \quad (12)$$

The mean of the temperatures measured by the four thermocouples on the heater (Fig. 1) was used for the heater temperature $T_w(x,y,0)$ in the central region (with a diameter 15 cm). A 2 to 3° lower temperature was used for $T_w(x,y,0)$ near the edge (Fig. 2b). Calculations show that 1° variation in $T_w(x,y,0)$ near the edge results in about 0.2% variation of total thermal conductivity. The mean of the temperatures measured by the four thermocouples on the cold plate (Fig. 1) was used for the $T_w(x,y,L_z)$.

Equations (6), (10a–f) and (12) are solved numerically using the finite difference method to determine the solid conductivity, k_c, and the temperature distribution. The finite-difference form of equation (6) is

$$A(i,j,k)\left[\left(\frac{T(i+1,j,k)-T(i-1,j,k)}{2\Delta x}\right)^2 + \left(\frac{T(i,j+1,k)-T(i,j-1,k)}{2\Delta y}\right)^2 + \left(\frac{T(i,j,k+1)-T(i,j,k-1)}{2\Delta z}\right)^2\right] + [B(i,j,k)+k_c] \times \left[\frac{T(i+1,j,k)-2T(i,j,k)+T(i-1,j,k)}{(\Delta x)^2} + \frac{T(i,j+1,k)-2T(i,j,k)+T(i,j-1,k)}{(\Delta y)^2} + \frac{T(i,j,k+1)-2T(i,j,k)+T(i,j,k-1)}{(\Delta z)^2}\right]=0. \quad (13)$$

The estimates of solid conductivity and temperature distribution in the medium are assumed and then $A(x,y,z)$ and $B(x,y,z)$ [equation (5a)], a_R [equation (7)] and q_r [equation (8)] are calculated. Solving equations (13), (10a–f) and (12) yields a new temperature distribution and solid conductivity. The procedure is

Table 2. Summary of data of five measurements

Parameter	Test 1	Test 2	Test 3	Test 4	Test 5
Voltage, V	4.8420	5.4365	5.8887	6.4679	7.2300
Current, A	0.2938	0.3219	0.3437	0.3698	0.4431
Power, W	1.4219	1.7495	2.0231	2.3910	3.2025
T_{heater}, °C	30.06	59.91	79.83	99.86	29.98
T_{plate}, °C	10.22	40.23	60.16	80.13	10.03
T_{mean}, °C	20.10	50.03	69.97	89.96	20.00
Pressure, Torr	0.2	0.4	0.7	1.0	760.0
k [equation (4)], mW m^{-1} K^{-1}	6.39	7.94	9.20	10.85	14.38
k [equation (13)], mW m^{-1} K^{-1}	6.50	8.27	9.77	11.70	14.49
k_c, mW m^{-1} K^{-1}	4.55	5.01	5.35	5.86	12.55
k_r, mW m^{-1} K^{-1}	1.94	3.25	4.41	5.84	1.94
a_R, m^2 kg^{-1}	41.23	32.88	28.95	25.91	41.29

then repeated using the obtained new temperature distribution and spatially averaged solid conductivity. The mesh sizes used in the numerical simulation are: $\Delta x = 0.5$, $\Delta y = 0.5$ and $\Delta z = 0.05$ cm. Finer mesh sizes changed the results by less than 0.1%. The iteration accuracy for the temperatures is 0.01 K and for the solid conductivity is 0.01 mW m^{-1}·K^{-1}. The spatial variation of the solid conductivity calculated from equation (12) is less than 0.5%.

RESULTS AND DISCUSSION

Four experiments were conducted at mean temperatures of about 20, 50, 70 and 90°C with the gas pressure below 1 Torr. Gas conduction is negligible at this pressure [9, 10]. Another measurement was made at one atmosphere at a mean temperature of 20°C (cf. Table 2).

For one-dimensional transfer, the total (apparent) thermal conductivity is given by

$$k_{app} = (Q/2F)\cdot\delta/\Delta T = (IV/2F)\cdot\delta/\Delta T,$$
$$\Delta T = T_{heater} - T_{plate}. \quad (14)$$

The results for k_{app} using equation (14) are listed in Table 2 and shown in Fig. 3.

Test 1 has the lowest gas pressure and the lowest mean temperature among the five tests (Table 2). The uncertainty of, k_{app}, has the largest value for test 1 and is analyzed below. The precision limit, $P_{k_{app}}$ is [11]

$$\frac{P_{k_{app}}}{k_{app}} = \sqrt{\left[\left(\frac{P_I}{I}\right)^2 + \left(\frac{P_V}{V}\right)^2 + \left(\frac{P_\delta}{\delta}\right)^2 + \left(\frac{P_F}{F}\right)^2 + \left(\frac{P_{\Delta T}}{\Delta T}\right)^2\right]}$$
$$= \sqrt{\left[\left(\frac{0.0001\text{ amp.}}{0.2938\text{ amp.}}\right)^2 + \left(\frac{0.002\text{ volt}}{4.842\text{ volt}}\right)^2 + \left(\frac{0.024\text{ cm}}{1.160\text{ cm}}\right)^2 + \left(\frac{0.5\text{ cm}^2}{645.0\text{ cm}^2}\right)^2 + \left(\frac{0.40\text{ K}}{19.84\text{ K}}\right)^2\right]}$$
$$= 0.029.$$

The bias limit, $B_{k_{app}}$, is

$$\frac{B_{k_{app}}}{k_{app}} = \sqrt{\left[\left(\frac{B_I}{I}\right)^2 + \left(\frac{B_V}{V}\right)^2 + \left(\frac{B_\delta}{\delta}\right)^2 + \left(\frac{B_F}{F}\right)^2 + \left(\frac{B_{\Delta T}}{\Delta T}\right)^2\right]}$$
$$= \sqrt{\left[\left(\frac{0.0001\text{ amp.}}{0.2938\text{ amp.}}\right)^2 + \left(\frac{0.002\text{ volt}}{4.842\text{ volt}}\right)^2 + \left(\frac{0.048\text{ cm}}{1.16\text{ cm}}\right)^2 + \left(\frac{0.5\text{ cm}^2}{645.0\text{ cm}^2}\right)^2 + \left(\frac{0.44\text{ K}}{19.84\text{ K}}\right)^2\right]}$$
$$= 0.047.$$

The overall uncertainty in the determination of k_{app}, $U_{k_{app}}$, is

$$\frac{U_{k_{app}}}{k_{app}} = \sqrt{\left[\left(\frac{P_{k_{app}}}{k_{app}}\right)^2 + \left(\frac{B_{k_{app}}}{k_{app}}\right)^2\right]}$$
$$= \sqrt{(0.029^2 + 0.047^2)} = 0.055.$$

The results from the three-dimensional analysis are listed in Table 2 and are shown in Fig. 3. The temperature of the heater is higher near the center than near the edge (Fig. 2b); the cold plate has a uniform temperature. Thus, the temperature difference and the heat flux near the center are larger than the average values. Using this higher temperature difference and the total (average) heat flux (from the heater) results in a k_{app} [using equation (14)] that is smaller than

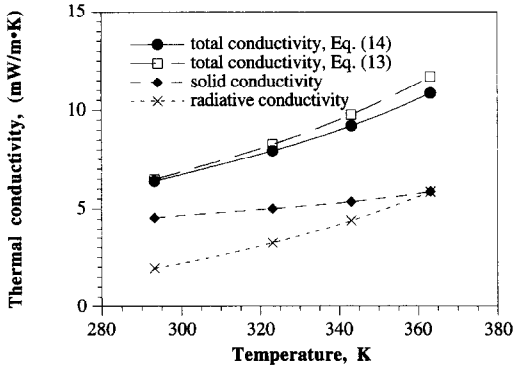

Fig. 3. Temperature dependence of thermal conductivity of carbon doped silica aerogel.

the k_{app} that is obtained from the three-dimensional analysis. At 20°C, k_{app} from the one-dimensional analysis is 1.7% smaller than that from the three-dimensional analysis; at 90°C, they differ by 7.3%. As the temperature increases, the heat loss increases and the assumption of one-dimensional heat transfer is less accurate. For materials other than the aerogel, the edge heat loss would be different and the difference between one-dimensional analysis and the three-dimensional analysis would also be different. Generally, a radiation-participating material with a lower absorption coefficient will have a larger edge heat loss due to the radiative transfer, and one-dimensional analysis will introduce a larger error.

A major advantage of the thin-film-heater thermal conductivity apparatus is its simplicity in realizing one-dimensional heat transfer. Figure 2 shows that the heater has a uniform temperature in the central region where the temperature is needed for one-dimensional calculation, and has only 2–3°C lower temperature near the edge. The cold plate has a very uniform temperature. Therefore, one-dimensional assumption can be used in the central region. To realize one-dimensional heat transfer, a thermal conductivity apparatus with guarded hot plates is much more complicated [12]. The guarded heaters are used around a main heater and insulation is needed outside the guarded heater. In addition to the complex system, longer time is needed to reach a thermodynamic equilibrium, and it is more difficult to conduct an uncertainty analysis.

The solid and radiative conductivities of aerogel are temperature dependent. It can be seen from Fig. 3 that the solid conductivity varies with temperature more slowly than the radiative conductivity does. At 20°C, the radiative conductivity is one-half of the solid conductivity; at 90°C, both conductivities are almost equal. At high temperatures, radiative heat transfer becomes more important and more carbon would be needed to reduce the radiative transfer.

The Rosseland absorption coefficient of silica aerogel (Table 2) decreases with temperature. At room temperature, the blackbody emissive power has a maximum at 9 μm where silica aerogel is highly opaque. As the temperature increases, the maximum of the blackbody emissive power shifts to shorter wavelengths where silica aerogel is less opaque. For the opacified aerogel used in the experiment, the Rosseland absorption coefficient is about 41 $m^2 kg^{-1}$ at 20°C and 26 $m^2 kg^{-1}$ at 90°C.

CONCLUSIONS

A thin-film-heater apparatus was developed for the measurement of the thermal conductivity. The apparatus uses a gold film heater of about 10 nm thickness coated on polyester. The thin heater results in a compact apparatus with small edge loss of heat.

Tests were carried out on opacified silica aerogel. Assuming one-dimensional heat transfer, the uncertainty of the measurement is 4.5%. A three-dimensional analysis is used to evaluate the validity of the assumption of one-dimensional heat transfer. The results show that the assumption of one-dimensional heat transfer results in a reduction in thermal conductivity of 1.7% at 20°C and a 7.3% reduction at 90°C.

The separate solid and radiative contributions were also obtained using the three-dimensional analysis. The solid conductivity of silica aerogel varies with temperature more slowly than the radiative conductivity does.

The Rosseland absorption coefficient of silica aerogel decreases with temperature. The sample used has a Rosseland absorption coefficient of about 41 $m^2 kg^{-1}$ at 20°C and 26 $m^2 kg^{-1}$ at 90°C.

Acknowledgements—This work was supported by the Assistant Secretary for Conservation and Renewable Energy, Advanced Industrial Concepts (AIC) Materials Program of the Advanced Industrial Concepts Division, Office of Industrial Technologies of the U.S. Department of Energy under contract no. DE-AC03-76F00098.

REFERENCES

1. N. E. Hager Jr, Recent developments with thin-heater thermal conductivity apparatus. In *Guarded Hot Plate and Heat Flow Meter Methodology*, ASTM STP 879 (Edited by C. J. Shirtliffe and R. P. Tyre), pp. 180–190. American Society for Testing and Materials, Philadelphia (1985).
2. D. L. McElroy, R. S. Graves, D. W. Yarbrough and J. P. Moore, A flat insulation tester that uses an unguarded nichrome screen wire heater. In *Guarded Hot Plate and Heat Flow Meter Metholodgy*, ASTM STP 879 (Edited by C. J. Shirtliffe and R. P. Tye), pp. 121–139. American Society for Testing and Materials, Philadelphia (1985).
3. A. J. Hunt, K. Jantzen and W. Cao, Aerogel—a high performance insulating material at 0.1 bar. In: *Insulation Materials: Testing and Applications*, ASTM STP 1116 (Edited by R. S. Graves and D. C. Wysocki), Vol. 2, pp. 455–463. American Society for Testing and Materials, Philadelphia (1991).
4. ASTM C 177-85, Standard test method for steady-state heat flux measurements and thermal transmission properties by means of the guarded-hot-plate apparatus. In *Annual Book of Standards*, pp. 20–31. American Society for Testing and Materials, Philadelphia (1985).
5. R. Siegel and J. R. Howell, *Thermal Radiation Heat Transfer* (2nd Edn), p. 689. Hemisphere, New York (1981).
6. J. S. Q. Zeng, R. Greif, P. Stevens, M. Ayers, and A. Hunt, Effective optical constants n and κ and extinction coefficient of silica aerogel, *J. Mater. Res.* **11**, 1–7 (1996).
7. M. Brewster, *Thermal Radiative Transfer and Properties*, pp. 443–444. Wiley, New York (1992).
8. Y. S. Touloukian, P. E. Liley and S. C. Saxena, *Thermophysical Properties of Matter*, Vol. 9. Plenum, New York (1970).
9. S. Q. Zeng, A. J. Hunt, W. Cao and R. Greif, Pore size distribution and apparent gas thermal conductivity of silica aerogel, *ASME J. Heat Transfer* **116**, 756–759 (1994).
10. S. Q. Zeng, A. J. Hunt and R. Greif, Mean free path and apparent thermal conductivity of a gas in a porous medium, *ASME J. Heat Transfer* **117**, 758–761 (1995).
11. Editorial, *Journal of Heat Transfer* policy on reporting uncertainties in experimental measurements and results, *J. Heat Transfer* **115**, 5–6 (1993).
12. G. S. Sheffield and J. R. Schorr, Comparison of thermal diffusivity and thermal conductivity methods, *Ceramic Bull.* **70**, 102–106 (1991).